Crystal structure, magnetic and electrical properties of $CaCu_3Mn_{4-x}Ti_xO_{12}$ ($0.3 \leq x \leq 3.0$) perovskites

2006 J. Phys.: Condens. Matter 18 6841

(http://iopscience.iop.org/0953-8984/18/29/021)

J. Phys.: Condens. Matter **18** (2006) 6841–6852 doi:10.1088/0953-8984/18/29/021

Crystal structure, magnetic and electrical properties of $CaCu_3Mn_{4-x}Ti_xO_{12}$ ($0.3 \leqslant x \leqslant 3.0$) perovskites

H Falcón[1], **J A Alonso**[1,3], **J Sánchez-Benítez**[2] **and M J Martínez-Lope**[1]

[1] Instituto de Ciencia de Materiales de Madrid, CSIC Cantoblanco, E-28049 Madrid, Spain
[2] Centre for Science at Extreme Conditions and School of Engineering and Electronics, University of Edinburgh, King's Buildings, Mayfield Road, Edinburgh EH9 3JZ, UK

Received 24 March 2006, in final form 8 June 2006
Published 6 July 2006
Online at stacks.iop.org/JPhysCM/18/6841

Abstract
The effect of substituting Ti for Mn in the ferrimagnetic perovskite $CaCu_3Mn_4O_{12}$ has been studied in the series $CaCu_3Mn_{4-x}Ti_xO_{12}$ ($x = 0.3, 0.5, 1.0, 1.5, 2.0, 3.0$). These materials have been prepared in polycrystalline form under moderate pressure conditions of 2 GPa and 1000 °C in the presence of $KClO_4$ as an oxidizing agent. The crystal structure is cubic, space group $Im\bar{3}$ (No. 204); the unit cell parameters vary linearly from $\mathbf{a} = 7.2361(4)$ Å ($x = 0.3$) to $\mathbf{a} = 7.3489(5)$ Å ($x = 3.0$) at room temperature (RT). A neutron powder diffraction study has been performed for a selected sample of nominal composition $CaCu_3Mn_3TiO_{12}$. In the ABO_3 perovskite superstructure, the A positions are occupied by Ca^{2+} and $(Cu^{2+}_{2.5}Mn^{3+}_{0.5})$, ordered in a 1:3 arrangement, giving rise to the body-centring of the unit cell. At the B positions, Mn and Ti are randomly distributed over the octahedral sites; $(Mn, Ti)O_6$ octahedra are considerably tilted by 19°, due to the relatively small size of the A-type cations. The Curie temperatures decrease from 331 K ($x = 0.3$) to 310 K ($x = 3.0$). The saturation magnetization at 5 K is strongly reduced upon Ti introduction, from $M_s = 10.4\ \mu_B\ fu^{-1}$ ($x = 0.3$) to $1.0\ \mu_B\ fu^{-1}$ ($x = 3.0$). All the samples exhibit negative magnetoresistance (MR), reaching a maximum value of 41% for the $x = 0.5$ sample at 5 K for $H = 9$ T; the MR(9 T) at RT is as high as 7% for $x = 0.5$, and shows an appreciable temperature stability.

(Some figures in this article are in colour only in the electronic version)

M Supplementary data files are available from stacks.iop.org/JPhysCM/18/6841

1. Introduction

Since the report of colossal magnetoresistance (MR) properties in hole-doped manganese perovskites of composition $La_{1-x}A_xMnO_3$, very few oxide systems have been described to

[3] Author to whom any correspondence should be addressed.

show these appealing properties, simultaneously exhibiting ferromagnetic and half-metallic character [1]. Besides the simple oxides CrO_2 and Fe_3O_4, some selected complex oxides such as the pyrochlore $Tl_2Mn_2O_7$ or the double perovskite Sr_2FeMoO_6 and substituted derivatives have been demonstrated to show non-negligible MR at room temperature, as required for technological applications [2].

Recently, the complex perovskite $CaCu_3Mn_4O_{12}$ [3, 4] has attracted the interest of solid-state scientists, since it exhibits a considerable low-field magnetoresistance at room temperature, decoupled with T_C (355 K). $CaCu_3Mn_4O_{12}$ was first reported by Chenavas *et al* [5]. The crystal structure of $CaCu_3Mn_4O_{12}$ has the originality of containing Cu^{2+} (or other Jahn–Teller transition metal cations, such as Mn^{3+}) at the A positions of the ABO_3 perovskite; this Jahn–Teller cation and Ca^{2+} are 3:1 ordered in a $2\mathbf{a}_0 \times 2\mathbf{a}_0 \times 2\mathbf{a}_0$ cubic cell of $Im\bar{3}$ symmetry (where $\mathbf{a}_0$ = unit cell of the perovskite aristotype). This perovskite is strongly distorted, showing an important tilting of the MnO_6 octahedra, given the small size of the cations at the A positions. Density functional calculations [6] show that $CaCu_3Mn_4O_{12}$ is a spin-asymmetric ferrimagnetic semiconductor, where Cu spins are antiferromagnetically coupled to Mn magnetic moments and the existence of a spin-dependent gap implies a thermally induced transport that is 100% polarized.

The flexibility of this structural type, of general formula $AA'_3B_4O_{12}$, has been demonstrated to be high concerning the different cationic substitutions that it is able to accommodate. A is generally a large monovalent or divalent or rare-earth cation; A′ is Cu^{2+} or Mn^{3+}; and B can be $Mn^{4+/3+}$, Ti^{4+}, Ru^{4+}, or Ge^{4+} [7, 8]. For instance, the replacement of Ca^{2+} cations by rare earths in the $RCu_3Mn_4O_{12}$ family (where R = rare earths), implies an electron doping effect that affects the magnetic and transport properties, as demonstrated recently [9, 10]. Also, Cu^{2+} can be replaced by another Jahn–Teller-like cation, typically Mn^{3+}, in the series $CaCu_{3-x}Mn_{4+x}O_{12}$ [4, 11].

The preparation of $CaCu_3Mn_4O_{12}$ and other compounds of the $AA'_3B_4O_{12}$ family has been described to require high-pressure conditions (7 GPa), necessary to stabilize the small A cations in the 12-fold positions of the perovskite. Recently, we have been able to synthesize well-crystallized (polycrystalline) samples of some new derivatives of $CaCu_3Mn_4O_{12}$ at moderate pressures of 2 GPa, starting from very reactive precursors obtained by wet-chemistry procedures, in the presence of $KClO_4$ as an oxidizing agent [12, 13].

On the other hand, when B = Ti^{4+}, completely different but also very appealing properties have been described for $CaCu_3Ti_4O_{12}$ [14–17]: this compound has also attracted much attention since the recent report of a high dielectric constant (∼10.000 at 1 kHz) by Subramanian *et al* [14]. Normally, high dielectric constants are found in ferroelectric materials; however, this Ti phase does not show any evidence of ferroelectric behaviour or any phase transitions. It is also cubic, with the same space group and crystallographic features as $CaCu_3Mn_4O_{12}$, including a strong tilting of the TiO_6 octahedra. It has been reported to show a semiconducting behaviour, the origin of which is not well understood; it could be either an intrinsic mechanism or an extrinsic mechanism associated with departures from ideal stoichiometry [17].

In this work we have undertaken the study of the $CaCu_3(Mn_{4-x}Ti_x)O_{12}$ solid solution. It is expected that, upon departure from $CaCu_3Mn_4O_{12}$ by replacing Mn^{4+} by non-magnetic Ti^{4+} cations, a progressive reduction of magnetization and conductivity is realized, but the consequences for the magnetoresistance are not evident, since a slight phase separation of Ti-rich phases in the grain boundary could enhance extrinsic, low-field magnetoresistance for certain compositional ranges. This paper reports on the structural, magnetic and magnetotransport properties of some selected oxides for x = 0.3, 0.5, 1.0, 1.5, 2.0 and 3.0.

2. Experimental details

$CaCu_3Mn_{4-x}Ti_xO_{12}$ ($x = 0.3, 0.5, 1.0, 1.5, 2.0$ and 3.0) materials were obtained as black polycrystalline powders by a chemical route using citrates as precursors. Stoichiometric amounts of analytical grade $CaCO_3$, $Cu(NO_3)_2{\cdot}3H_2O$, and $MnCO_3$ were dissolved in citric acid. The solution was slowly evaporated, leading to an organic resin which was dried at 120 °C. The sample was then heated at 600 °C for 12 h in order to eliminate all the organic materials and nitrates. This precursor was thoroughly ground with the stoichiometric amount of TiO_2 and $KClO_4$ (30% in weight), put into a gold capsule (8 mm diameter; 10 mm length), sealed, and placed in a cylindrical graphite heater. The reaction was carried out in a piston–cylinder press (from Rockland Research Co.) at a hydrostatic pressure of 2 GPa at 1000 °C for 60 min. Then the material was quenched to room temperature and the pressure was subsequently released. The *in situ* decomposition of $KClO_4$ provides the high O_2 pressure required to stabilize Mn^{4+} cations. A fraction of the raw product, obtained as a dense, homogeneous pellet, was partially ground to perform the structural and magnetic characterization; some as-grown pellets were kept for magnetotransport measurements. The ground product was washed in a dilute HNO_3 aqueous solution, in order to dissolve KCl coming from the decomposition of $KClO_4$ and to eliminate small amounts of unreacted CuO; then the powder sample was dried in air at 150 °C for 1 h.

The characterization by XRD was performed using a Bruker-AXS D8 diffractometer (40 kV, 30 mA), controlled by DIFFRACT^{plus} software, in the Bragg–Brentano reflection geometry with Cu Kα radiation ($\lambda = 1.5418$ Å). A secondary graphite monochromator allowed the complete removal of Cu Kβ radiation. The data were obtained between 10 and 100° 2θ in steps of 0.05°. A neutron powder diffraction (NPD) pattern for a selected sample of composition $CaCu_3Mn_3TiO_{12}$ was acquired at the high-flux D20 diffractometer of the Institut Laue–Langevin in Grenoble (France). The sample, weighing 1 g, was packed in a vanadium holder of 6 mm diameter. The pattern was collected at room temperature with a wavelength of 1.31 Å and a counting time of 1 h in the high-resolution mode. The NPD pattern was analysed by the Rietveld method, using the FULLPROF program [18]. The line shape of the diffraction peaks was generated by a pseudo-Voigt function, and the background was refined to a fifth-degree polynomial. The coherent scattering lengths for Ca, Cu, Mn, Ti and O were, respectively, 4.70, 7.718, −3.73, −3.438 and 5.803 fm. In the final run, the following parameters were refined: background coefficients, zero-point, half-width, pseudo-Voigt and asymmetry parameters for the peak shape; scale factor, positional and occupancy factors for oxygens; thermal isotropic factors for all the atoms; and unit-cell parameters.

The dc magnetic susceptibility was measured using a commercial superconducting quantum interference device (SQUID) magnetometer on powdered samples, in the temperature range 5–400 K; transport and magnetotransport measurements were performed using the conventional four-probe technique, under magnetic fields of up to 9 T in a PPMS system from Quantum Design.

3. Results and discussion

$CaCu_3Mn_{4-x}Ti_xO_{12}$ oxides were obtained as black, well-crystallized powders. The laboratory XRD diagrams are shown in figure 1. The patterns are characteristic of cubic perovskites showing sharp, well-defined superstructure reflections due to the 1:3 ordering of Ca and Cu cations, and can all be indexed in the $Im\bar{3}$ space group. The unit-cell parameters are listed in table 1. A regular increase in the a unit-cell parameter is observed along the series, which can be

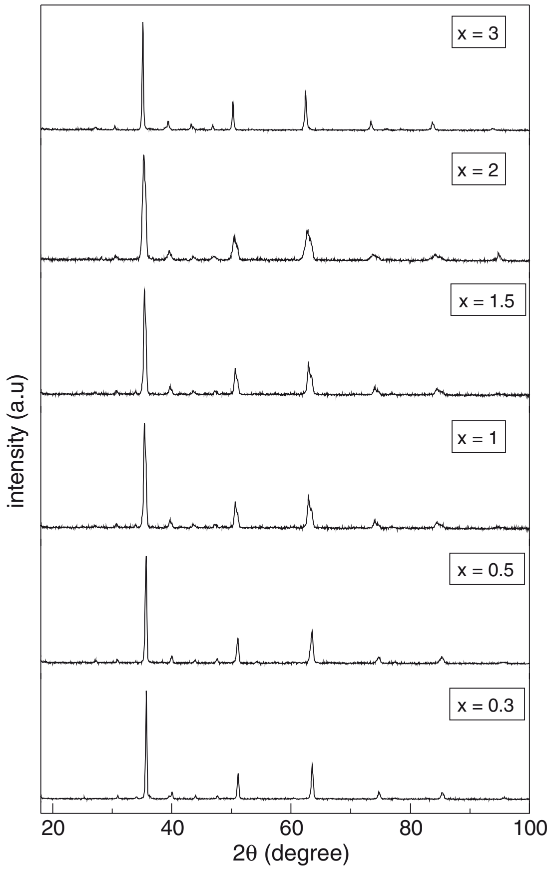

Figure 1. XRD patterns for $CaCu_3Mn_{4-x}Ti_xO_{12}$ ($x = 0.3, 0.5, 1.0, 1.5, 2.0, 3.0$).

Table 1. Unit-cell parameters and magnetic and magnetotransport constants of the perovskites $CaCu_3Mn_{4-x}Ti_xO_{12}$.

x	0.0[a]	0.3	0.5	1.0	1.5	2.0	3.0
a (Å)	7.227 93(5)	7.2361(4)	7.2432(6)	7.2650(9)	7.283(1)	7.305(1)	7.3489(5)
V (Å^3)	377.608(5)	378.89	380.0	383.45	386.30	389.82	396.89
T_C (K)	345	331	325	330	325/253	322/210	310/100
M_s (μ_B fu^{-1})	10.2	10.4	9.0	7.5	6.0	3.8	1.0
MR (%) 5 K, 9 T	34	27	41	39	36	—	—
MR (%) 300 K, 9 T	7	7	6.5	6.0	4.5	4.5	1.0

[a] Taken from [12].

ascribed to the larger size of Ti^{4+} cations (0.605 Å) versus Mn^{4+} cations (0.53 Å) in octahedral coordination [19]. The reported parameter for the $x = 0$ compound [5], $a = 7.241$ Å, slightly deviates from the trend mentioned; the size of the unit cell of $Ca(Cu_{2.5}Mn_{0.5})Mn_4O_{12}$ ($a = 7.2279(1)$ Å [12]) offers a better comparison with the present series, since the presence of 0.5 Mn atoms at the Cu positions was also detected from NPD data, as described hereafter. The linear evolution of the **a** unit-cell parameter and volume is displayed in figure 2.

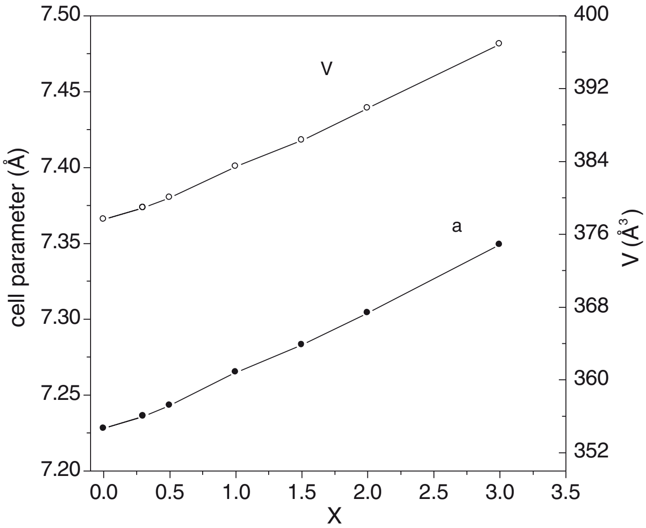

Figure 2. Variation of the **a** unit-cell parameter and volume with the Ti contents, x.

3.1. Structural refinement

The structural refinement was performed from RT NPD data for a selected sample of nominal composition $CaCu_3Mn_3TiO_{12}$ in the $Im\bar{3}$ (No. 204) space group, with a unit-cell parameter related to $\mathbf{a}_0$ (ideal cubic perovskite, $\mathbf{a}_0 \approx 3.8$ Å) as $\mathbf{a} \approx 2a_0$, using the $CaCu_3Mn_4O_{12}$ structure as a starting model [5], with Ca atoms at 2a (0, 0, 0) positions, Cu at 6b (0, 1/2, 1/2) positions, Mn and Ti distributed at random at 8c (1/4, 1/4, 1/4) and O at 24g $(x, y, 0)$ sites. A reasonable fit ($R_I \approx 6\%$) was obtained for this preliminary model. As a second step, the possibility that some Mn^{3+} cations occupy some of the Cu^{2+} positions at 6b sites was considered, and the complementary occupancy factors were refined, constrained to full occupancy. Neutron diffraction is specially suited to detect a small fraction of Mn at Cu positions, given the contrasting scattering lengths for both elements. After this refinement, the quality of the fit was notably improved, reaching a discrepancy factor of $R_I = 3.2\%$. The subsequent refinement of the occupancy factor for oxygen positions led to a slight deviation from the full stoichiometry. The crystallographic formula for this material resulted in being $Ca[Cu_{2.54(1)}Mn_{0.46(1)}]_{6b}$ $[Mn_3Ti]_{8c}$ $O_{11.6(1)}$. Assuming a valence of 2+ for Cu cations, 3+ for Mn at the 6b sublattice, and 4+ for Ti, the nominal valence for Mn at the 8c positions is 3.58(2)+. This average value corresponds to 58% Mn^{4+} and 42% Mn^{3+}. Table 2 includes the main atomic parameters and discrepancy factors after the refinement. Figure 3 shows the agreement between observed and calculated NPD profiles at RT. Table 3 contains a list of selected bond distances and angles.

The cubic perovskite superstructure of $CaCu_3Mn_{4-x}Ti_xO_{12}$, typified for $Ca(Cu_{2.5}Mn_{0.5})$ $(Mn_3Ti)O_{12}$, contains several features that must be highlighted. Ca atoms are coordinated to 12 oxygen atoms, with equal Ca–O distances of 2.56 Å, while the oxygen environment for (Cu^{2+}, Mn^{3+}) cations is highly irregular, with eight rather long distances (2.72 and 3.19 Å at RT) and an effective coordination number of four, with Cu–O bond-lengths of 1.945 Å in a pseudo-square arrangement (table 3). These CuO_4 units are not strictly square, exhibiting O–Cu–O angles of 94.8° and 85.2°. At the B substructure of the perovskite, (Mn^{4+}, Mn^{3+}, Ti^{4+}) cations occupy the centre of virtually regular octahedra, with (Mn, Ti)–O bond-lengths of 1.923(1) Å at

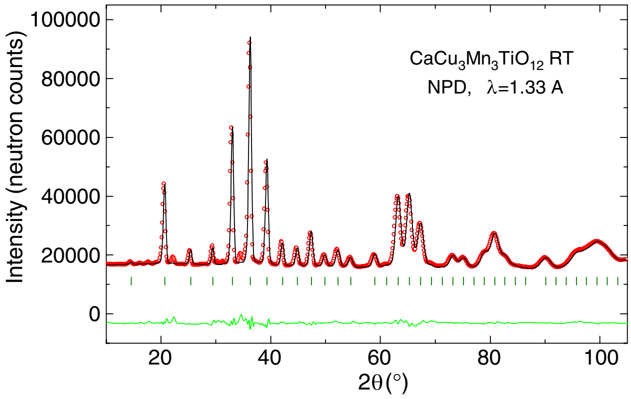

Figure 3. Observed (circles), calculated (full line) and difference (bottom) NPD Rietveld profiles for $CaCu_3Mn_3TiO_{12}$ at RT, collected at the high-flux D20-ILL diffractometer.

Table 2. Structural parameters for $CaCu_3Mn_3TiO_{12}$ refined in the cubic $Im\bar{3}$ space group at room temperature from NPD. (Lattice parameters: $\mathbf{a} = 7.265(1)$ Å and $V = 383.45$ Å^3. Discrepancy factors: $R_P = 1.34\%$, $R_{wp} = 2.00\%$, $R_{exp} = 0.70\%$, $\chi^2 = 8.24$ and $R_{Bragg} = 3.20\%$.)

Atom	Site	*x*	*y*	*z*	f_{occ}	*B* (Å^2)
Ca	2a	0.0000	0.0000	0.0000	1.0	0.6(1)
Cu	6b	0.0000	1/2	1/2	0.848(1)	0.17(7)
Mn	6b	0.0000	1/2	1/2	0.152(1)	0.17(7)
Mn	8c	1/4	1/4	1/4	0.75	0.42(7)
Ti	8c	1/4	1/4	1/4	0.25	0.42(7)
O	24g	0.3029(2)	0.1812(2)	0.0000	0.968(8)	0.41(3)

Table 3. Main bond distances (Å) and selected angles (degrees) for $CaCu_3Mn_3TiO_{12}$ determined from NPD data at RT.

CuO_{12} polyhedra	
Ca–O (×12)	2.564(1)
Cu–O (×4)	1.945(1)
Cu–O (×4)	2.7233(8)
Cu–O (×4)	3.195(1)
O–Cu–O	94.8(1)
O–Cu–O	85.2(1)
MnO_6 octahedra	
Mn–O (×6)	1.923(1)
O–Mn–O	90.29(7)
O–Mn–O	89.71(7)
Cu–O–Mn	108.85(5)
Mn–O–Mn	141.71(4)

RT. This distance is significantly longer than that observed for $CaCu_3Mn_4O_{12}$, of 1.915(1) Å [5] consistent with the incorporation of larger Ti^{4+} cations in the Mn^{4+} sublattice. A view of the crystal structure of $Ca(Cu_{2.5}Mn_{0.5})(Mn_3Ti)O_{12}$ is shown in figure 4. It is fairly distorted due to the small size of Ca^{2+} and Cu^{2+} cations, which force the (Mn, Ti)O_6 octahedra to tilt in order to optimize the Ca–O and Cu–O bond distances. The tilting angle of the octahedra can simply be derived from the (Mn, Ti)–O–(Mn, Ti) angle (141.7°) to be 19° at RT. It is remarkable

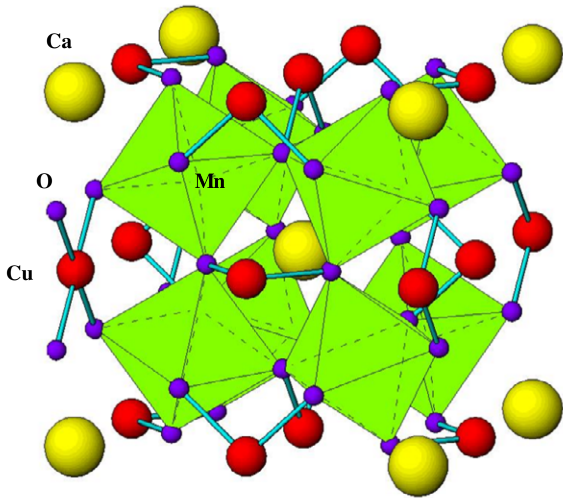

Figure 4. View of the structure of $CaCu_3Mn_{4-x}Ti_xO_{12}$. The **c** axis is vertical; the **a** axis is from right to left. Large, medium and small spheres represent Ca, Cu, and O, respectively; the square-planar coordination of Cu is highlighted. Corner-sharing $(Mn, Ti)O_6$ octahedra are fairly tilted in the structure to optimize Ca–O and Cu–O bond-lengths.

that, despite the increment in size of the $(Mn, Ti)O_6$ octahedra with respect to the undoped compound, which would suggest a decrease in the tolerance factor of the perovskite structure and, hence, an increment in the tilting effect of the octahedra, we observe a virtually unchanged Mn–O–Mn angle (142° for $CaCu_{2.5}Mn_{0.5}Mn_4O_{12}$ [12]). In this peculiar superstructure of perovskite, the tilting angle of the octahedral units is strongly determined by the CuO_4 square-planar units, in such a way that an increment in the octahedral size is accommodated by an expansion of the CaO_{12} and CuO_4 units, which are, in this case, under a certain tensile stress.

3.2. Magnetic and electrical properties

The magnetization versus temperature curves shown in figure 5 exhibit the abrupt increase characteristic of a spontaneous ferromagnetic ordering. The spontaneous magnetization corresponds to the opposite alignment of Cu_{6b} and Mn_{8c} magnetic moments. The Curie temperatures can be determined from the inflection in the magnetization curves. The T_C s for $CaCu_3Mn_{4-x}Ti_xO_{12}$ are 331 K ($x = 0.3$), 325 K ($x = 0.5$), 330 K ($x = 1.0$), 325 K ($x = 1.5$), 322 K ($x = 2.0$) and 310 K ($x = 3.0$), progressively decreasing from that observed in the undoped ferrimagnetic system $Ca(Cu_{2.5}Mn_{0.5})Mn_4O_{12}$ ($T_C = 345$ K) [12]. As shown in the inset of figure 5, the $x = 3.0$ compound shows a distinct behaviour, exhibiting a much less abrupt magnetization increment below T_C. The inflections observed in the curves for $x = 1.5, 2.0$ and 3.0, at the temperatures indicated in table 1, could be ascribed to a certain phase segregation, as will be commented on below. The magnetization versus magnetic field isotherms collected at $T = 5$ K shown in figure 6 also exhibit a saturation magnetic moment which decreases along the series, as 10.4, 9.0, 7.5, 6.0, 3.8 and 1.0 μ_B fu^{-1} for $x = 0.3, 0.5, 1.0, 1.5, 2.0, and 3.0$, respectively. It is clear that the introduction of non-magnetic Ti^{4+} cations weakens the magnetic interactions and diminishes the total magnetic moment at the B positions of the perovskite, leading to the observed reduction in the Curie temperature and the saturation magnetization. To understand the observed values of saturation magnetization, we can take the example of the $x = 1.0$ compound, for which the NPD data

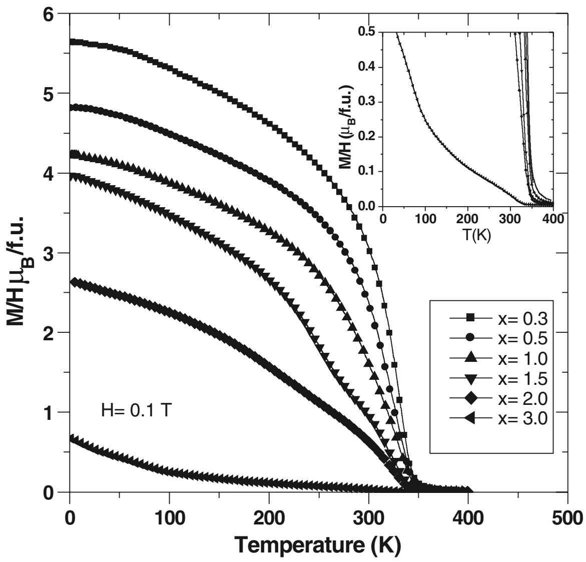

Figure 5. Temperature dependence of the dc magnetic susceptibility. The inset is a close-up showing the onset of long-range ferrimagnetic interactions, below T_C.

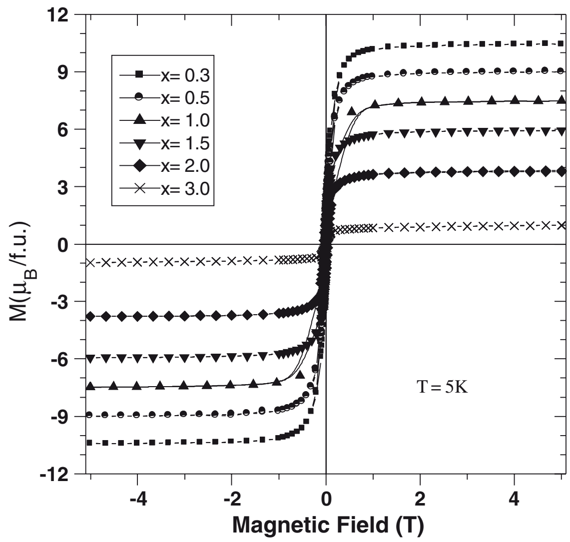

Figure 6. Magnetization isotherms at $T = 5$ K for $CaCu_3Mn_{4-x}Ti_xO_{12}$.

have demonstrated partial occupancy of Mn^{3+} cations at Cu^{2+} positions. Previous studies of the magnetic structure for $Ca(Cu_{2.5}Mn_{0.5})_{6b}Mn_{8c}O_{12}$ [12] showed that the Cu^{2+} moments are antiferromagnetically coupled to the Mn_{8c} spins, giving a global ferrimagnetic structure, whereas the Mn^{3+} spins at 6b positions adopt an almost perpendicular direction to Cu^{2+} moments and, therefore, do not contribute to the global magnetization. In our case, assuming the same spin configuration for the perovskite $Ca(Cu_{2.5}Mn_{0.5})_{6b}(Mn^{3+}_{1.26}Mn^{4+}_{1.74}Ti^{4+})_{8c}O_{12}$, and considering a contribution of 1 μ_B for spin-only Cu^{2+} ($S = 1/2$), 4 μ_B for Mn^{3+} and 3 μ_B

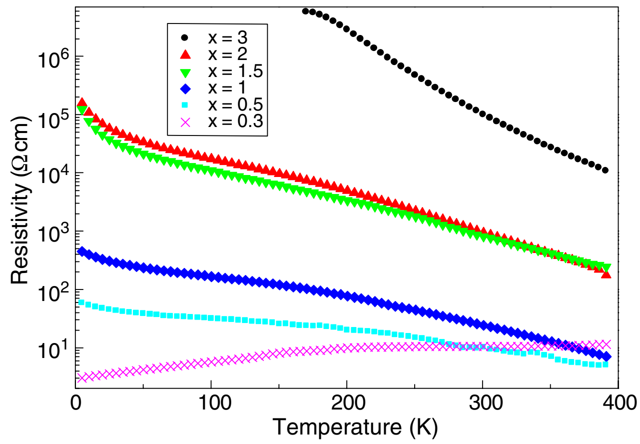

Figure 7. Resistivity versus temperature curves for $CaCu_3Mn_{4-x}Ti_xO_{12}$.

for Mn^{4+}, we would obtain a net magnetization of 7.76 μ_B fu^{-1}, in good agreement with the observed value of 7.5 μ_B fu^{-1}

It is worth commenting that, whereas the magnetization diminishes by about ten times from $x = 0.3$ to 3.0, the Curie temperature decrease by less than 10% through the concentration range studied. This situation is not unique and has been observed in different ferrimagnetic systems where the magnetic atoms are diluted with non-magnetic atoms, leading to a dramatic reduction in the global magnetization, depending linearly on the concentration of the magnetic cation, but undergoing a minor perturbation of the strength of the magnetic interactions. In this case, these interactions are not merely the superexchange coupling between Mn spins within the B sublattice, certainly spoiled by the introduction of non-magnetic Ti^{4+} cations, but are mediated by the Cu spins at the A sublattice, since the Cu–O–Mn magnetic coupling is hardly hindered by the presence of Ti^{4+} at the B positions of the perovskite. An additional example of ferrimagnetic systems with large T_C s and poor saturation magnetizations are given by the family of double perovskites $Sr_3Fe_2B'O_9$ ($B' =$ W, Mo, U) [20–22], where the intrinsic disordering of Fe and B′ cations over the B positions of the perovskite drastically reduces the global ferrimagnetic moment but does not perturb the strong antiferromagnetic interactions between neighboring Fe spins.

Figure 7 shows the resistivity versus temperature plots for the samples with different Ti doping levels, x. Except for $x = 0.3$, which shows a positive slope characteristic of metallic behaviour, the resistivity for all samples increases with cooling, exhibiting a semiconducting behaviour. As the Ti content rises, the resistivity increases over the whole temperature range by several orders of magnitude. For low doping levels ($0.3 \leqslant x \leqslant 1.0$) it is worth highlighting that the observed value for $\rho(T = 300\text{ K})$, of around 10^2 Ω cm, is considerably smaller than that of $\sim 1.8 \times 10^3$ Ω cm described for the parent $CaCu_3Mn_4O_{12}$ compound [3]. This low resistivity value suggests an increase in the carrier density with respect to the parent compound, probably related to the mixed valence state induced on the Mn cations at the B positions of the perovskite as a consequence of the partial occupancy of Mn^{3+} at the Cu^{2+} sites. This effect is particularly important for the $x = 0.3$ compound, which presents a metal-like temperature dependence of resistivity, in contrast to the rest of compounds, including the parent oxide $CaCu_3Mn_4O_{12}$; for increasing doping levels, this effect is largely counteracted by the introduction of Ti^{4+} (d^0), progressively draining the electrons at the conduction band. It is worth mentioning that all the pellets used for the transport measurements contain about 30% KCl, coming from the

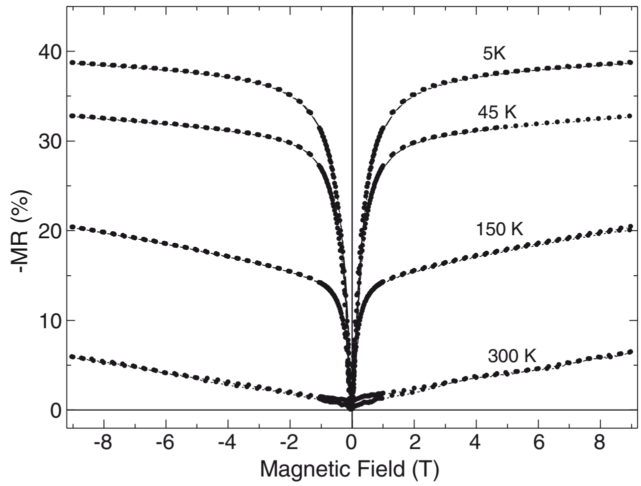

Figure 8. Magnetoresistance (MR, in %) isotherms for $CaCu_3Mn_3TiO_{12}$. MR is defined as $100 \times [R(9\ T) - R(0)]/R(0)$.

decomposition of $KClO_4$ during the synthesis process and a small fraction of unreacted CuO; however, since the amount of these insulating impurities is well below the percolation limit, we believe its presence has little influence on the transport properties compared to the huge changes described above, ascribable to electronic effects.

Regarding the changes in resistance under a magnetic field, we define $MR(H) = 100 \times [R(H) - R(0)]/R(0)$. Figure 8 illustrates the evolution of MR versus the magnetic field as isotherms at selected temperatures in the $H = 0$–9 T range for $CaCuMn_3TiO_{12}$. The magnetoresistance increases with decreasing temperature, reaching a maximum value of -39% at 5 K and 9 T. At 300 K there is a non-negligible magnetoresistance of -6% at 9 T. The most striking feature of these isotherms is the strong component of low-field MR, defined for magnetic fields lower than 1 T. A value of MR(1 T) higher than 33% is observed at 5 K, and it is non-negligible (about 2%) at RT. These figures make this compound a candidate for applications in spintronics devices.

Similar measurements have been recorded for the remaining phases; the plots are available as supplementary information at stacks.iop.org/JPhysCM/18/6841. The MR values exhibited for the different Ti doping levels are listed in table 1, for $T = 5$ and 300 K. It is surprising that, despite the smooth and continuous decrease in T_C along the series, MR(5 K) slightly increases and reaches a maximum for $x = 0.5$, and then decreases for higher doping levels. The fact that MR in these materials is not related to the Curie temperature suggests a mechanism of spin-polarized inter-grain tunnelling [23, 24]. We can conceive two mechanisms that account for the increment in magnetoresistance with x in the low-doping region. From the point of view of the intrinsic magnetotransport properties, the increase in resistance at low temperatures could be ascribed to a reduction in the net number of carriers in the system upon Ti^{4+} doping. Recently, Majumdar and Littlewood [25] demonstrated that there is a relationship between the MR and the reciprocal of the charge carrier density (n), according to the equation $MR = C(M/M_s)^2$, where M_s is the saturation magnetization and C is proportional to $n^{-2/3}$. In the high Ti-doping region, the concomitant degradation of the magnetic properties, involving a dramatic decrease in the net magnetization (see figure 6), would account for the observed decay in MR for the last members of the series.

From the point of view of the extrinsic MR, it is plausible that a small phase segregation in Ti-rich regions, undetectable by diffraction methods, could create additional boundaries that may enhance the extrinsic low-field magnetoresistance. Finally, from the preparative point of view, it is worth commenting that, although in the present work all the compounds of the series have been synthesized under the same moderate-pressure conditions of 2 GPa, for the sake of comparison, it is almost certain that the samples with higher Ti contents would require lower pressures to be stabilized, since the term of the series, $CaCu_3Ti_4O_{12}$, can be prepared under ambient pressure [16]. The reduction of the synthesis pressure for intermediate compounds with enhanced MR is an additional advantage to the possible application of the materials of the $CaCu_3Mn_4O_{12}$ family in spintronic devices.

4. Conclusions

Six oxides of the series $CaCu_3Mn_{4-x}Ti_xO_{12}$ ($x = 0.3, 0.5, 1.0, 1.5, 2.0, 3.0$) with a perovskite-related structure have been synthesized at a moderate pressure of 2 GPa in the presence of an oxidizing agent. The structural refinement from RT NPD data for a selected sample with $x = 1.0$ shows that the 6b positions of the perovskite are randomly occupied by Cu^{2+} and Mn^{3+} cations; the magnetization measurements suggests that Cu^{2+}_{6b} and $(Mn^{3+}, Mn^{4+})_{8c}$ moments are antiferromagnetically aligned, giving rise to a global ferrimagnetic structure. The tilting angle of the (Mn, Ti)O_6 octahedra does not significantly evolve from the undoped compound, in spite of the expansion of the octahedral units, since the tilting is strongly determined by the CuO_4 square-planar units. The magnetic interactions smoothly decrease along the series, resulting in lower T_C s and saturation magnetizations upon Ti^{4+} introduction. The resistivity increases along the series; this fact is ascribable to the reduction in the number of carriers and, for moderate Ti-doping levels, this fact boosts the intrinsic magnetoresistance, according to the Majumdar–Littlewood model [25]. The extrinsic, low-field MR is also enhanced for low Ti contents, despite the decrease in T_C, which could be a consequence of moderate phase segregation in Ti-rich regions, promoting compositional boundaries where the spin-dependent scattering is improved.

Acknowledgments

H Falcón is grateful to the Secretaría de Estado de Educación y Universidades for a grant received. Financial support from the Spanish CICyT, under Project MAT2004-0479, and from the Comunidad de Madrid to the Project GR/MAT/0427/2004 is acknowledged. We are grateful to the Institut Laue–Langevin for making all facilities available.

References

[1] Ramirez A P 1997 *J. Phys.: Condens. Matter* **9** 8171
[2] Ziese M 2002 *Rep. Prog. Phys.* **65** 143
[3] Zeng Z, Greenblatt M, Subramanian M A and Croft M 1999 *Phys. Rev. Lett.* **82** 3164
[4] Zeng Z, Greenblatt M, Sunstrom J E, Croft M and Khalid S 1999 *J. Solid State Chem.* **147** 185
[5] Chenavas J, Joubert J C, Marezio M and Bochu B J 1975 *J. Solid State Chem.* **14** 25
[6] Weth R and Pickett W E 2001 *Phys. Rev.* B **65** 14415
[7] Bochu B, Joubert J C, Collomb A, Ferrand B and Samaras D 1980 *J. Magn. Magn. Mater.* **15** 1319
[8] Deschizeaux M N, Joubert J C, Vegas A, Collomb A, Chenavas J and Marezio M 1976 *J. Solid State Chem.* **19** 45
[9] Alonso J A, Sánchez-Benítez J, de Andrés A, Martínez-Lope M J, Casais M T and Martínez J L 2003 *Appl. Phys. Lett.* **83** 2623

[10] Sánchez-Benítez J, Alonso J A, de Andrés A, Martínez-Lope M J, Casais M T and Martínez J L 2004 *J. Magn. Magn. Mater.* **272** 1407
[11] Troyanchuk I O, Lobanovsky L S, Kasper N V, Hervieu M, Maignan A, Michel C, Szymczak H and Szewczyk A 1998 *Phys. Rev.* B **58** 14903
[12] Sánchez-Benítez J, Alonso J A, Martínez-Lope M J, Casais M T, Martínez J L, de Andrés A and Fernández-Díaz M T 2003 *Chem. Mater.* **15** 2193
[13] Sánchez-Benítez J, Alonso J A, Falcón H, Martínez-Lope M J, de Andrés A and Fernández-Díaz M T 2005 *J. Phys.: Condens. Matter* **17** S3063
[14] Subramanian M A, Li D, Duan N, Reisner B A and Sleight A W 2000 *J. Solid State Chem.* **151** 323
[15] Subramanian M A and Sleight A W 2002 *Solid State Sci.* **4** 347
[16] Jha P, Arora P and Ganguli A K 2003 *Mater. Lett.* **57** 2443
[17] West A R, Adams T B, Morrison F D and Sinclair S C 2004 *J. Eur. Ceram. Soc.* **24** 1439
[18] Rodríguez-Carvajal J 1993 *Physica* B **192** 55
[19] Shannon R D 1976 *Acta Crystallogr.* A **32** 751
[20] Ivanov S A, Eriksson S-G, Tellgren R and Rundlof H 2001 *Mater. Res. Bull.* **36** 2585
[21] Viola M C, Alonso J A, Pedregosa J C and Carbonio R E 2005 *Eur. J. Inorg. Chem.* 1559
[22] Pinacca R M, Viola M C, Pedregosa J C, Carbonio R E and Alonso J A 2005 *J. Mater. Chem.* **15** 4648
[23] Hwang H Y, Cheong S-W, Ong N P and Batlogg B 1996 *Phys. Rev. Lett.* **77** 2041
[24] Kobayashi K-I, Kimura T, Sawada H, Terakura K and Tokura Y 1998 *Nature* **395** 677
[25] Majumdar P and Littlewood P 1998 *Nature* **395** 479